The Formation of Kelvin-Helmholtz Instabilities on Swirling Axisymmetric Vortex Rings

C.L. Gargan-Shingles[1], M. Rudman[1], and K. Ryan[1]

[1]Department of Mechanical and Aerospace Engineering
Monash University, Victoria 3800, Australia

Abstract

The dynamics induced by the inclusion of a swirl component in a vortex ring have yet to be fully described. The development of a region of negatively signed vorticity at the leading edge of a vortex core has been observed for swirling rings in both numerical simulations and laboratory experiments, by various authors.

In this paper, a spectral element method is used to solve the axisymmetric Navier-Stokes equations for swirling vortex rings with a Gaussian initial condition. A Kelvin-Helmholtz instability is shown to develop within the negative vorticity region at the leading edge of the rings. Vortex rings with ratios varying between 0.2 and 0.5 are considered, with swirl magnitudes from 0.0 to 0.5. The initial circulation Reynolds numbers for all cases is 10 000.

A cut-off shear Reynolds number has been defined, above which vortex rings of negative vorticity are formed by the instability, and subsequently ejected from the system. Shear layers weaker than this threshold fail to produce the secondary rings. The strain rate within the original core is shown to fluctuate during the ejection process, due to the superposition of the strain fields present in the system. The results of this study allow predictions of Gaussian ring behaviour to be made given a set of initial conditions.

Introduction

Vortex rings with swirl are common in most transitional and turbulent flows, and are considered to be essential building blocks of such flows [18]. The study of vortex rings with a swirling velocity component may enhance our knowledge of bubble-type vortex breakdown [12], the breakdown of tip vortices on delta wings [14], and give insight into the behaviour of helical vortices [5], which can be found in the downwash of helicopter blades [1]. Naitoh *et al.* [10] found that swirl is generated in the core of non-swirling vortex rings due to Kelvin instabilities. This suggests that all vortex rings can have a localized induced swirl component at some stage in their evolution.

A common simplification used in numerical analyses of vortex rings is to assume that the core has a Gaussian distribution of azimuthal vorticity. However, a Gaussian vorticity distribution is only an exact steady solution of the Navier-Stokes equations for infinitely thin cores. Hence, a numerical vortex ring with a finite sized core will evolve from the initial Gaussian distribution towards a new equilibrium state over time, a process known as relaxation [15].

The axial velocity strength W of a swirling vortex ring can be expressed via

$$W = \frac{2\pi a}{\Gamma}\overline{u_\theta},$$ (1)

where $\overline{u_\theta}$ is the maximum axial velocity through the core, Γ is the core circulation, and a is the radius of the vortex core. The size or thickness of a vortex ring can be expressed through the ring radii ratio Λ, where, if R is the radius of the ring,

$$\Lambda = \frac{a}{R}.$$ (2)

The growth of a region of oppositely signed vorticity at the leading edge of a swirling vortex ring has been shown by various authors [3, 11, 12, 18]. At high swirls (W > 1.0), this region immediately forms into a secondary vortex ring, which overpowers the original ring [3]. At lower swirls, however, the region remains at the leading edge as a shear layer [12]. Shear layer instabilities, such as the Kelvin-Helmholtz instability (KHI), have previously been observed in the formation structures of vortex rings by Glezer [4], and later Lim [8]. It has been found that the KHI plays an important role in triggering the transition from a laminar vortex ring to a turbulent vortex ring [8].

In shear layers consisting of a unidirectional flow of fluid, the velocity profile must have an inflexion point to be unstable to small wavy disturbances [13]. This instability mechanism is inviscid, and will only be damped out by the presence of viscosity [9]. It is known that the shorter the wavelength of the instability, the higher the amplification of the corresponding unstable mode. However, in reality, the wavelength of the most amplified instability will be close to the width of the shear layer [13]. This paper will elucidate the growth of a KHI from within the shear layer of a swirling vortex ring, and outline the effect that the initial conditions have on its development.

Methodology

The cross section of the vortex core is initially defined by a Gaussian distribution of azimuthal vorticity ω_θ, and a Gaussian distribution of azimuthal velocity u_θ. They are non-dimensionalised and expressed in cylindrical polar co-ordinates (z, r, θ) using the initial circulation Γ_0, initial core size a_0, initial ring radius R_0, the initial swirl number W_0, and a radial coordinate centred on the vortex core s, giving

$$\omega_\theta = 2e^{-s^2},$$ (4)

$$\text{and } u_\theta = W_0 e^{-s^2}.$$ (5)

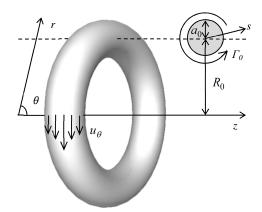These parameters are shown graphically in Figure 1.

Figure 1. Schematic of the axisymmetric coordinate system for a swirling ring. R_0, a_0, Γ_0, and v_θ are flow parameters, while z, r, θ, and s are coordinate descriptors. The vorticity and swirl profiles of the vortex core are both initially Gaussian.

The initial flow field is defined using the three orthogonal cylindrical velocity vectors. The u_r and u_z components are found by solving the streamfunction equation, given by

$$\omega_\theta = \frac{\partial^2 \Psi}{\partial z^2} - \frac{\partial}{\partial r}\left(\frac{1}{r}\frac{\partial r\Psi}{\partial r}\right). \qquad (6)$$

The governing equations are solved using a spectral element method, which discretises a spatial domain into small elements over which a high degree polynomial basis is applied [6]. The partial differential equations being solved are recast as integral equations, which can be converted to a set of ordinary differential equations through approximation by Gauss-Legendre-Lobatto quadrature. The numerical code used here was first demonstrated by Sheard *et al.* [16], while the 2D axisymmetric solver was developed by Sheard and Ryan [17]. For these simulations, 11th order polynomials are used, on a mesh with a grid spacing of $0.25a_0$ in the region near to the vortex core. The overall size of the domain is $400a_0 \times 200a_0$. A grid resolution study has been performed, confirming that the results obtained are within 2% of the grid independent results.

The time t is related to the dimensional time t_s through

$$t = \frac{t_s}{2\pi} \times \frac{\Gamma_0}{a_0^2}. \qquad (7)$$

Additionally, two different definitions of Reynolds numbers are used to describe the ring properties. The first defines the overall flow field, using the kinematic viscosity v, through

$$Re = \frac{\Gamma}{v}. \qquad (8)$$

The second describes the strength of the shear layer, using the shear layer width δ and velocity differential ΔV over the width, through the relation

$$Re_s = \frac{\delta \Delta V}{v}. \qquad (9)$$

The circulation, ring radius, and core radius, for each case, are obtained by following the analysis used in Archer *et al.* [2]. The shear layer is identified by first determining the velocity magnitude along a line which both intersects the point of peak negative vorticity, and is tangent to the direction of the local vorticity contours. The width δ is defined as the length of a segment of this line, containing the peak negative vorticity, over which the velocity gradient is significantly negative (magnitude less than 5% of ω_θ at $t = 0$).

Simulations are performed for 96 cases, using 16 values of Λ_0 (from 0.2 to 0.5) and 6 values of W_0 (0.0 to 0.5). Each simulation is initialised with $Re = 10\,000$, and is run for 100 time units.
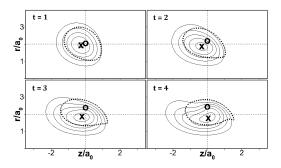

Figure 2. Contours (solid lines) of u_θ overlaid with a measure of the core radius a (dashed line). Contours separated by 0.10. The x indicates the position of maximum swirl magnitude. The o indicates the position of the maximum vorticity magnitude.
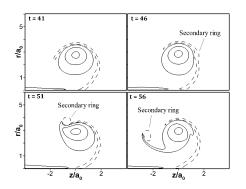

Figure 3. Contours of ω_θ for the core of the vortex ring, showing growth of the KHI. Contours displayed are -0.25, 0.10, 1.10, 2.10.

Results and Analysis

Through the initial stages of the evolution, the shape of the ω_θ field within the vortex core warps as it relaxes towards the steady solution of the governing equations. This influences the shape of the swirl contours, as shown in Figure 2.

As the shape of the core evolves, the leading edge develops a concentrated region of negative vorticity near the axis of the ring. This negative vorticity region at the leading edge is effectively a unidirectional shear layer containing an inflection point of velocity. Over time, it is wrapped around the leading edge of the core (shown as the dotted line contour in Figure 3). It is from within this region that the KHI develops, producing a secondary vortex ring, with negative vorticity (see Figure 3).

The core radius size fluctuates early in the evolution due to the relaxation process. The core relaxation time is thus defined as the instant at which the core radius reaches a plateau after this initial period of change. The time in which this levelling out occurs varies with Λ_0, as shown in Figure 4. It also varies significantly with W_0 for $\Lambda_0 > 0.3$. The measured ring radius R at the relaxation time shows a similar trend, as shown in Figure 5. For $\Lambda_0 < 0.3$, the magnitude of the swirl present in the ring has little effect on the size of the ring radius at the time of core relaxation.

Next, we consider the strength of the shear layer, defined using the shear Reynolds number from equation (9), for cases in which it has a measurable growth. The shear Reynolds number is monitored over time, and reaches an initial peak in magnitude for all cases, at which time its value is recorded. An estimate for the time of initial growth of the secondary ring due to the KHI instability is obtained by monitoring the r-position of the peak negative vorticity at the leading edge of the vortex core.
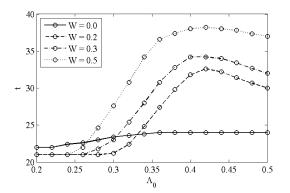
Figure 4. Time required for core relaxation for various combinations of Λ_0 and W_0. Lines have been shown for clarity purposes. Uncertainty in each point is of the order of ± 1.
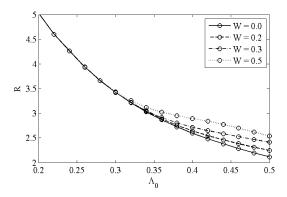

Figure 5. Ring radius size at the core relaxation time for various combinations of Λ_0 and W_0. Lines have been shown for clarity purposes. Uncertainty in each point is of the order of ± 1.

A relationship between the sampled shear Reynolds number and the initial ring conditions has been determined, and has the form

$$Re_s \propto \log_e(W_0 \Lambda_0^3). \qquad (10)$$

The raw data used to develop this expression is shown in Figure 6; a clear linear relationship can be seen.

The various combinations of parameters can be separated into three groups, based on their Re_s. In cases for which $Re_s < 200$, the secondary ring has not been observed to form for any case. For shear layers with $Re_s > 250$, the secondary ring is always observed in some form. The absence of the secondary ring in the lower Re_s cases can be attributed to the KHI either being prematurely damped out, or simply being too weak to generate the secondary ring. Additionally, shear layers that are too short in length may not permit growth of the KHI wavelengths. Typically, rings of larger Λ_0 have longer shear layers.

For any ring below the zero contour line, it is predicted that no noticeable shear layer will form. Figure 7 shows the relationship between the core relaxation time, the time to the initial peak in Re_s, and the time of initial generation of the secondary ring (defined as the instant before the position of peak negative vorticity begins to move away from the z-axis). Thicker rings (larger Λ_0) tend to take longer to relax, and reach their maximum shear Reynolds number faster. Although not presented here, rings with larger swirl magnitudes show a similar trend.
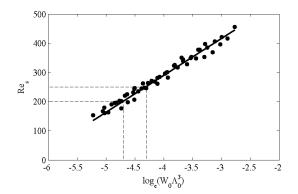

Figure 6. Dependence of Re_s on Λ_0 and W_0. Linear relationship determined empirically from numerical data. Cases less than 200 will produce a shear layer but no secondary ring. Cases greater than 250 will produce both a shear layer and the secondary ring.
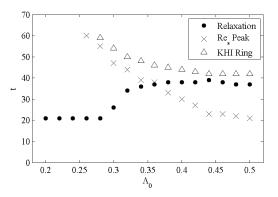

Figure 7. Comparison of the time frames required for vortex core relaxation, initial peak in Re_s, and growth of the secondary ring, for $W_0 = 0.5$. Other values of W_0 show similar trends and so have not been presented here.

The key observation from Figure 7 is that the secondary ring produced by the KHI is not evident until the conditions around the vortex core have relaxed, and the initial peak in Re_s has been reached. The KHI ring timing curve in Figure 7 closely follows that of the Res curve for low Λ_0, and the Re_s curve for high Λ_0, suggesting that the secondary ring cannot grow until the core has relaxed fully.

The KHI also influences the internal strain rate (or ε_{int}, as defined in [7]) of the vortex core. As the instability forms the secondary ring (e.g. $t = 41$ in Figure 3), there is a local maximum in the magnitude of the internal strain rate over time. The secondary ring moves gradually around the original ring, with a corresponding decrease in the strain rate, before the strain rate returns to a local maximum as the secondary ring reaches its largest radius (e.g. just before $t = 51$ in Figure 3). This maximum is a result of the superposition of the opposing induction velocities of the original and secondary rings.

Finally, the secondary ring is ejected into the wake, resulting in another local minimum. This process repeats for each secondary ring that forms, taking between 15 and 25 time units to complete one cycle. The change in the strain rate over time is presented in Figure 8, with the shaded sections each representing a single cycle.
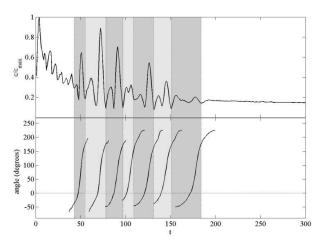
Figure 8. Top: Development of the internal strain rate, ε, over time, normalized by its maximum value. The first region represents the initial relaxation, while the subsequent shaded regions are negative vorticity ejections due to the KHI. The final region shows the settling of the internal strain rate as viscous diffusion becomes dominant. Bottom: Relative position of the core of each secondary ring with respect to the core of the primary ring, over time. Angle measured from positive z-axis.

In the final stage of evolution, the core strain rate settles down to a relatively steady value, once the shear layer has insufficient strength to generate any further vortices. The evolution of the ring at this stage is governed only by viscous diffusion. The settling of the strain rate can also be seen in Figure 8.

Conclusions

A swirling axisymmetric vortex ring with a Gaussian initial distribution of azimuthal vorticity was analysed using a spectral element method, in order to investigate the development of a Kelvin-Helmholtz instability from the shear layer at the leading edge. The core of the Gaussian ring was found to numerically relax to a new equilibrium state of the Navier-Stokes equations in a time period that was dependent on both Λ_0 and W_0 for rings with $\Lambda_0 > 0.3$.

A region of negative ω_θ was seen to develop at the leading edge of the ring, and reached an initial maximum in a time frame which was inversely proportional to both Λ_0 and W_0. The strength of this region, represented by the shear Reynolds number, was found to be proportional to $\log_e(W_0\Lambda_0^3)$. The KHI was found to produce an oppositely signed vortex ring from within the shear layer in all cases where $Re_s > 250$, and no cases where $Re_s < 200$.

It was also noted that the secondary ring would only form after both the Re_s had reached a local maximum and the core had relaxed sufficiently towards a steady solution of the Navier-Stokes equations. The presence of the KHI was shown to influence the strain rate within the vortex core, preventing the core from reaching a diffusive-only state until shear layer was too weak to support the continued growth of the instability. Additional research needs to be undertaken to determine the effect of altering the overall Reynolds number, and the flow dynamics for cases with $W_0 > 0.5$.

References

[1] Ahlin, G.A. & Brown, R.E., Wake Structure and Kinematics in the Vortex Ring State, *Journal of the American Helicopter Society*, **54,** 2009.

[2] Archer, P.J., Thomas, T.G., & Coleman, G.N., Direct numerical simulation of vortex ring evolution from the laminar to the early turbulent regime, *Journal of Fluid Mechanics*, **598,** 2008, 201-226.

[3] Cheng, M., Lou, J., & Lim, T.T., Vortex ring with swirl: A numerical study, *Physics of Fluids*, **22,** 2010.

[4] Glezer, A., The formation of vortex rings, *Physics of Fluids*, **31,** 1988.

[5] Hattori, Y. & Fukumoto, Y., Effects of axial flow on the stability of a helical vortex tube, *Physics of Fluids*, **24,** 2012.

[6] Karniadakis, G. & Sherwin, S., Spectral/hp Element Methods for Computational Fluid Dynamics. 1999: Oxford University Press.

[7] Le Dizes, S. & Laporte, F., Theoretical predictions for the elliptical instability in a two-vortex flow, *Journal of Fluid Mechanics*, **471,** 2002, 169-201.

[8] Lim, T.T., On the role of Kelvin-Helmholtz-like instability in the formation of turbulent vortex rings, *Fluid Dynamics Research*, **21,** 1997.

[9] Michalke, A., On the inviscid instability of the hyperbolic-tangent velocity profile, *Journal of Fluid Mechanics*, **19,** 1964, 543-556.

[10] Naitoh, T., *et al.*, Experimental study of axial flow in a vortex ring, *Physics of Fluids*, **14,** 2002, 143-149.

[11] Naitoh, T., *et al.*, On the evolution of vortex rings with swirl, *Physics of Fluids*, **26,** 2014.

[12] Ooi, A., *et al.* A Numerical Study of Swirling Vortex Rings. in *Australiasian Fluid Mechanics Conference: 14AFMC*, Adelaide University, 2001,375-378.

[13] Rayleigh, L., On the stability, or instability, of certain fluid motions, *Proceedings of the London Mathematical Society*, **1,** 1880, 474-487.

[14] Shariff, K. & Leonard, A., Vortex Rings, *Annual Review of Fluid Mechanics*, **24,** 1992, U235-U279.

[15] Shariff, K., Verzicco, R., & Orlandi, P., A numerical study of three-dimensional vortex ring instabilities: viscous corrections and early nonlinear stage, *Journal of Fluid Mechanics*, **279,** 1994, 351-375.

[16] Sheard, G.J., *et al.*, Flow around an impulsively arrested circular cylinder, *Physics of Fluids*, **19,** 2007.

[17] Sheard, G.J. & Ryan, K., Pressure-driven flow past spheres moving in a circular tube, *Journal of Fluid Mechanics*, **592,** 2007, 233-262.

[18] Virk, D., Melander, M.V., & Hussain, F., Dynamics of a Polarized Vortex Ring, *Journal of Fluid Mechanics*, **260,** 1994, 23-55.